European Journal of Neuroscience, Vol. 18, pp. 344–354, 2003

Cell type-dependent expression of HCN1 in the main olfactory bulb

Noémi B. Holderith,[1] Ryuichi Shigemoto[2] and Zoltan Nusser[1]
[1]Laboratory of Cellular Neurophysiology, Institute of Experimental Medicine, Hungarian Academy of Sciences, Szigony Street 43, 1083 Budapest, Hungary
[2]Division of Cerebral Structure, National Institute for Physiological Sciences, Okazaki, Japan

Keywords: immunogold, immunohistochemistry, olfaction, periglomerular cells, rat

Abstract

In many brain regions, hyperpolarization-activated cationic currents (I_h) are involved in the generation of rhythmic activities, but the role of I_h in olfactory oscillations remains unclear. Knowledge of the cellular and subcellular distributions of hyperpolarization-activated and cyclic nucleotide-gated channel (HCN) subunits is necessary for understanding the role of I_h in olfactory network activities. Using light microscopic immunocytochemistry, we demonstrate strong HCN1 labelling of the glomerular layer and moderate staining of granule cell, internal and external plexiform layers of the rat main olfactory bulb. In the glomerular layer, among many unlabelled neurons, two distinct subpopulations of juxtaglomerular cells are labelled. Approximately 10% of the juxtaglomerular cells strongly express HCN1. These small diameter cells are immunoreactive for GABA and comprise a subpopulation of periglomerular cells. An additional subset of juxtaglomerular cells ($\approx$ 1%) expresses low levels of HCN1. They are large in diameter, GABA immunonegative but immunopositive for vesicular glutamate transporter 2, characterizing them as external tufted cells. Quantitative immunogold localization revealed that the somatic plasma membranes of periglomerular cells contain approximately four times more HCN1 labelling than those of external tufted cells. Unlike in cortical pyramidal cells, immunogold density for HCN1 does not significantly differ in somatic and dendritic plasma membranes of external tufted cells, indicating that post-synaptic potentials arriving at proximal and distal dendrites are modulated by the same density of I_h. Our results demonstrate a cell type-dependent expression of HCN1 in the olfactory bulb and predict a differential contribution of distinct juxtaglomerular cell types to network oscillations.

Introduction

In the CNS, hyperpolarization-activated cationic currents (I_h) through hyperpolarization-activated and cyclic nucleotide-gated channels (HCN) are involved in a large variety of functions, including the generation of rhythmic activities, modulation of firing properties of nerve cells, setting the resting membrane potential and integration of synaptic inputs (Pape, 1996; Magee, 2000; Accili *et al.*, 2002). For example, dendritic I_h plays a critical role in attenuating the location dependence of temporal integration of excitatory synaptic potentials in hippocampal and neocortical pyramidal cells. To achieve this, a non-uniform somato-dendritic distribution of I_h is required, which has been demonstrated by several groups (Schwindt & Crill, 1997; Magee, 1998; Stuart & Spruston, 1998; Williams & Stuart, 2000; Berger *et al.*, 2001). The involvement of I_h in spontaneous rhythmic contraction of the heart and in generation of thalamic oscillations during the sleep–wake cycle has also been demonstrated (Pape & McCormick, 1989). Oscillations have been described in many other brain regions (Singer, 1999; Buzsaki, 2002), including the olfactory bulb (Adrian, 1942, 1950; Freeman, 1975, 1976; Laurent & Davidowitz, 1994), but the underlying cellular and molecular mechanisms and the involvement of I_h are not fully understood in this brain area. In order to comprehend the possible role of I_h in olfactory network activities, it is necessary to determine the cellular and subcellular distributions of HCN subunits in the main olfactory bulb (MOB).

To date, four subunits (HCN1–4) of the HCN gene family have been cloned (Santoro *et al.*, 1997, 1998; Gauss *et al.*, 1998; Ludwig *et al.*, 1998; Monteggia *et al.*, 2000). Recent experiments suggest that the molecular heterogeneity of these channels is further increased by the formation of heteromultimeric assemblies of the four subunits (Chen *et al.*, 2001; Ulens & Tytgat, 2001). Functional properties of HCN channels, such as their activation and deactivation kinetics and their modulation by cyclic nucleotides, depend on the subunit compositions (Ludwig *et al.*, 1998; Moosmang *et al.*, 2001). However, not only the molecular structure but also the density and precise subcellular distribution of HCN subunits will determine the functional role of I_h (Schwindt & Crill, 1997; Magee, 1998, 1999; Williams & Stuart, 2000; Berger *et al.*, 2001). In cortical and hippocampal pyramidal cells, the cell surface distribution of HCN1 is remarkably complex and highly regulated. In a recent study, Lorincz *et al.* (2002) have demonstrated that, in neocortical, hippocampal and subicular pyramidal cell dendrites, the density of HCN1 increases as a function of distance from the soma. Furthermore, dendritic shafts had a significantly higher HCN1 content than spines at the same distance from the soma, revealing a subcellular compartment dependence of HCN1 density. In the present study, we also asked whether the above-mentioned features of the cell surface distribution of HCN1 are generally true for nerve cells or whether they are specific for cortical pyramidal cells. We have used light and electron microscopic immunolocalizations to

Correspondence: Dr Zoltan Nusser, as above.
E-mail: nusser@koki.hu

Received 3 April 2003, revised 8 May 2003, accepted 12 May 2003

doi:10.1046/j.1460-9568.2003.02756.x

reveal the cellular and subcellular distribution of HCN1 in the MOB and to quantitatively assess its densities in different subcellular compartments of distinct juxtaglomerular cell (JGC) types.

Materials and methods

Preparation of tissue

Eleven adult male Wistar rats were deeply anaesthetized with ketamine (30 mg/kg) and xylazine (10 mg/kg). They were perfused through the aorta with 0.9% saline for 1 min, followed by ice-cold fixatives. For pre-embedding peroxidase and immunofluorescence reactions, the animals were perfused with fixatives containing 4% paraformaldehyde, 0.05% glutaraldehyde and ~0.2% picric acid (five animals) and 4% paraformaldehyde and ~0.2% picric acid (six animals) made up in 0.1 M phosphate buffer (pH 7.4) for 25 min, respectively. Following fixations, the brains were quickly removed from the skull and placed in phosphate buffer. For pre-embedding immunogold reactions and post-embedding immunocytochemistry on semithin sections, five adult Wistar rats were perfused with fixatives containing 2% paraformaldehyde and 1% glutaraldehyde in 0.1 M sodium acetate buffer (pH 6) for 2 min followed by 1 h perfusion with 2% paraformaldehyde and 1% glutaraldehyde in 0.1 M borate buffer (pH 9; Sloviter *et al.*, 2001). The brains were left in the skull for 24 h at 4 °C prior to removal. Horizontal sections (60 µm thick) were cut from the olfactory bulb with a Vibratome (VT1000S; Leica Microsystems, Vienna, Austria), followed by several washes in phosphate buffer. Tissues fixed with 1% glutaraldehyde-containing fixatives were treated with 1% sodium borohydrate in phosphate buffer for 30 min prior to immunoreactions.

Pre-embedding immunoperoxidase reactions

Normal goat serum (NGS, 10%) in Tris-buffered saline (TBS, pH 7.4) was used for blocking, followed by incubations in the primary and secondary antibodies. Guinea pig (HCN1-Gp) and rabbit (HCN1-R; Alomone Laboratories, Jerusalem, Israel) polyclonal antibodies to HCN1 (Lorincz *et al.*, 2002) were diluted in TBS containing 2% NGS and 0.05% TritonX-100 at final concentrations of 1.4 and 4 µg/mL, respectively. Sections for immunoperoxidase reactions were incubated in biotinylated goat anti-guinea pig or goat anti-rabbit IgGs (Vector Laboratories, Burlingame, CA, USA; diluted 1 : 50 in TBS containing 2% NGS) for 3 h, followed by several washes and an incubation in 0.5% avidin-biotinylated horseradish peroxidase complex (ABC; Vector Laboratories) for 2 h. The enzyme reaction was revealed by 3′3-diaminobenzidine tetrahydrochloride (0.05% solution in TB) as chromogen and 0.01% H_2O_2 as oxidant.

Sampling and disector analysis

The percentage of HCN1-immunopositive cells in the JGC population was determined using the disector method (Gundersen, 1977). The glomerular layer of the olfactory bulb contains tightly packed JGC somata around the glomeruli, some of which showed HCN1 immunoreactivity. Large areas of the glomerular layer (containing at least five glomeruli) were randomly selected and cut out from sections reacted for HCN1 with the pre-embedding immunoperoxidase method (from three animals). Serial semithin sections (0.5 µm thick) were cut from each block. To prevent false HCN1-immunonegative cells due to the lack of penetration of immunoreagents into the depth of tissue during the pre-embedding reactions, semithin sections were cut only from the surface (top 5 µm) of the 60-µm-thick sections. Pairs of semithin sections (2 µm apart) were stained with toluidin blue and all nuclei of nerve cells were counted ($n = 3$ animals, 249 ± 48 in each animal). The disector distance (2 µm) was chosen according to the estimated smallest diameter of the HCN1-positive cells (5–6 µm). Disector analysis was performed on composite images ($\approx 1500 \times 200$ µm in each animal; original images taken with a DP50 CCD camera with a 40× objective; Olympus). Images were analysed in Photoshop 7.0 (Adobe Systems) and HCN1-immunopositive cells were marked on consecutive sections not stained for toluidin blue. The analysis was performed in both directions by interchanging the reference and look-up sections.

Post-embedding immunocytochemistry on semithin sections

Immunoreactivity for GABA in JGCs was revealed by a post-embedding method on semithin sections (Somogyi *et al.*, 1985). Semithin sections (0.5 µm thick) were cut from HCN1 immunoperoxidase-reacted and epoxy resin-embedded tissue and carefully dried onto gelatin-coated slides. The sections were then treated with sodium ethanolate (saturated sodium hydroxide solution in 100% ethanol) for 30 min followed by extensive washing in absolute ethanol and distilled water. The osmium was removed by treatment with a freshly prepared 1% $NaIO_4$ solution for 40 min. The slides were then washed in TBS, followed by blocking with 10% NGS in TBS for 30 min. Following blocking, the sections were incubated in drops of rabbit polyclonal antibody against GABA (GABA9, gift from Prof Peter Somogyi; diluted 1 : 2000 in TBS containing 2% NGS) for 2 h. The reaction was revealed with goat anti-rabbit IgG coupled to Cy3 (1 : 500; Jackson ImmunoResearch Laboratories, West Grove, PA, USA). The sections were then washed and mounted in Vectashield.

The fluorescent intensity, indicating the immunoreactive GABA content of the cells, was measured over the nuclei of each cell using Scion Image 4.0.2 (2000 Scion Corporation, Bethesda, MD, USA) following digital image-capturing with a DP50 camera (Olympus). The mean value was calculated for each cell ($n = 3$ animals, 464 ± 73 cells in each animal). The nuclei were chosen to measure GABA immunoreactivity because the 3′3-diaminobenzidine tetrahydrochloride precipitate in the cytoplasm of the HCN1-immunopositive cells masked the immunoreactive GABA molecules. Each cell/nucleus was also identified on adjacent toluidin blue-stained sections.

Double immunofluorescent reactions

For double fluorescent labelling, the following antibodies were used together with the HCN1-Gp: anti-calbindin D28k (1 : 1000 rabbit polyclonal or 1 : 1000 mouse monoclonal; Swant, Bellinzona, Switzerland), anti-calretinin (1 : 1000 mouse monoclonal; Swant), anti-tyrosine hydroxylase (TH; 1 : 5000 mouse monoclonal; ImmunoStar, Hudson, WI, USA), rabbit anti-vesicular glutamate transporter 1 (anti-vGluT1; 1 : 2500 rabbit polyclonal; Synaptic Systems, Göttingen, Germany) and anti-vGluT2 (1 : 500 rabbit polyclonal; Synaptic Systems). After several washes in TBS, sections were further incubated in a mixture of biotinylated goat anti-guinea pig (1 : 50 dilution; Vector Laboratories) and goat anti-rabbit or goat anti-mouse antibodies conjugated to Alexa-594 (1 : 500, highly cross-adsorbed; Molecular Probes, Leiden, the Netherlands) for 3 h. Following washing in TBS, the sections were incubated in 0.5% ABC solution for 2 h. The enzyme reaction was revealed by tyramide coupled to Oregon green 488 (Tyramide Signal Amplification Kit; Molecular Probes) as described by the manufacturer. This method was used to enhance the weak immunosignal in external tufted cells (ETCs). After several washes in buffer, the sections were mounted on slides in Vectashield (Vector Laboratories). No labelling could be detected when the guinea pig primary antibody was used with anti-rabbit or anti-mouse secondary antibodies or when the rabbit or mouse primary antibodies were reacted with anti-guinea pig secondary antibodies.

Quantitative evaluation of the double-labelling immunofluorescent reactions

Areas (321 × 238 μm) were randomly selected along the glomerular layer at both the lateral and medial sides of the MOB. Digital images (DP50 camera, 40× objective; Olympus) were taken from the surface of the sections to avoid potential false negativity due to differences in the penetration of the antibodies. Data are given as mean ±SD from three animals.

Pre-embedding immunogold reactions

Sections for immunogold reaction were incubated in HCN1-Gp (diluted in TBS + 2% NGS + 0.1% TritonX-100) overnight. After several washes in TBS, the sections were blocked in TBS containing 0.8% bovine serum albumin (Sigma) and 0.1% cold-water fish skin gelatin (Aurion Immunoresearch, Wageningen, the Netherlands) for 20 min. Sections were then incubated in goat anti-guinea pig IgG coupled to 0.8-nm gold particles (Aurion Immunoresearch) diluted 1 : 50 in the blocking solution overnight at 4 °C. Following several washes, the sections were fixed in a 1% glutaraldehyde solution (made up in TBS). After three 10-min washes in TBS and two 10-min washes in Enhancement Conditioning Solution (Aurion Immunoresearch), gold particles were silver enhanced using the R-Gent SE-LM Silver kit as described by the manufacturer (Aurion Immunoresearch).

Double immunogold and immunoperoxidase reactions

Sections for double immunogold and immunoperoxidase reactions were blocked and incubated in a mixture of the following primary antibodies: HCN1-Gp and vGluT2 (1 : 500; Synaptic Systems) and HCN1-Gp and anti-vesicular GABA transporter (1 : 2000; Chemicon, Temecula, CA, USA) as described above. After the incubation in primary antibodies, the sections were blocked in TBS containing 0.8% bovine serum albumin and 0.1% cold-water fish skin gelatin for 20 min. Sections were then incubated in a mixture of the following secondary antibodies: goat anti-guinea pig IgG coupled to 0.8-nm gold particles (Aurion Immunoresearch) and biotinylated goat anti-rabbit IgG (Vector Laboratories) for 6 h at 4 °C. Following several washes, the sections were fixed in a 1% glutaraldehyde solution (made up in TBS). After three 10-min washes in TBS and two 10-min washes in enhancement conditioning solution, gold particles were silver enhanced using the R-Gent SE-LM Silver kit. The sections were then further incubated in 0.5% ABC solution for 2 h, before the enzyme reaction was revealed by 3′3-diaminobenzidine tetrahydrochloride (0.05%) as chromogen and 0.01% H_2O_2 as oxidant.

Sections following pre-embedding immunoperoxidase and immunogold reactions were post-fixed in 0.5% OsO_4 for 20 min, stained in 1% uranyl acetate, dehydrated in graded series of ethanol and embedded into epoxy resin (Durcupan; Sigma).

No immunoreactivity could be detected when either the primary or the secondary antibodies were omitted or the sections were treated with the silver kit only.

Quantitative analysis of the immunogold reaction

To quantitatively compare HCN1 immunogold densities between two subpopulations of immunopositive JGCs and between distinct subcellular compartments of the cells, immunoreactive HCN1 was revealed with a pre-embedding immunogold method. With this method, immunoparticle density decreases as a function of distance from the surface into the depth of the tissue. Therefore, neuronal profiles were analysed within the first micrometre from the surface of the tissue. Digital images (MegaViewII camera) were taken from each area of interest from three serial sections (each two sections apart). In each tri-series of electron micrographs, labelled dendritic shafts, somata, axons and axon terminals were identified. The length of the plasma membranes and the area of the cytoplasm were measured (Analysis; Soft Imaging Systems, Munster, Germany). A gold particle was considered to be associated with the plasma membrane if the middle of the particle was within 46 nm of the middle of the lipid bilayer on the cytoplasmic side of the membrane (see Lorincz *et al.*, 2002). If the particle was further away from the membrane, it was considered as an intracytoplasmic gold particle. Non-specific (background) immunogold density was calculated over the nuclei of JGCs (Lorincz *et al.*, 2002). Immunoparticle densities (in particle/μm^2) were calculated in particle/effective membrane area (effective membrane area = membrane length × effective membrane width of 46 nm) over the labelled plasma membrane compartments (ETC somatic plasma membranes (SoMe), mitral/tufted cell dendritic plasma membranes (DeMe), periglomerular cell (PGC) SoMe and DeMe of all labelled dendrites). In two animals, immunoparticle densities over the above-mentioned plasma membrane and cytoplasmic compartments were statistically (unpaired *t*-test) compared with the non-specific labelling density measured over the nuclei of JGCs (also given in particle/μm^2). For the plasma membrane compartments, we also calculated the immunoparticle density in particle/membrane length following the subtraction of non-specific labelling density. Data are given as mean ±SEM. Mitral/tufted cell dendrites were identified as large, relatively empty profiles, establishing asymmetrical synaptic contacts onto other dendrites. Based on ultrastructural features, the distal dendrites of mitral and tufted cells cannot be distinguished and, therefore, we refer to them as mitral/tufted cell dendrites. Periglomerular cell bodies were identified upon their large nucleus : cytoplasm ratio, relatively heterochromatic nucleus and very few cytoplasmic organelles. External tufted cells were identified as relatively large cells (8–15 μm), with euchromatic nucleus, relatively large cytoplasm with elaborate ER and Golgi apparatus and occasionally making somato-dendritic asymmetrical synapses onto dendritic profiles. Only labelled profiles were included in the analysis with the criterion that at least one membrane-associated particle was present in any of the three sections of the profile.

Results

Distribution of HCN1 immunoreactivity in the main olfactory bulb

The regional, cellular and subcellular distribution of HCN1 immunoreactivity was investigated with two polyclonal antibodies raised against two, non-overlapping sequences of the protein (rabbit anti-HCN1, HCN1-R, amino acid residues 6–24; guinea pig anti-HCN1, HCN1-Gp, amino acid residues 850–910). The specificity of the antibodies was described previously (Lorincz *et al.*, 2002). Similarly to the neocortex and hippocampal formation, the two antibodies revealed practically identical cellular and subcellular distribution patterns for HCN1 in the MOB, with somewhat stronger staining provided by the HCN1-Gp antibody. Because of this, the detailed quantitative analysis of HCN1 immunoreactivity in the MOB was carried out using the HCN1-Gp antibody. In the MOB, the strongest labelling for HCN1 was detected in the glomerular layer, whereas the internal and external plexiform layers and the granule cell layer were moderately labelled (Fig. 1A). In the plexiform layers, diffuse neuropil labelling for HCN1 was observed, without detectable immunoreactivity in somata and main apical and lateral dendritic processes of mitral cells, internal- and middle-tufted cells (Fig. 1E). In the granule cell layer, a few weakly labelled cells were found with morphological features reminiscent of granule cells (Fig. 1F). The weak diffuse neuropil labelling of the granule cell layer and external plexiform layer probably originates from a low intensity labelling of granule cell

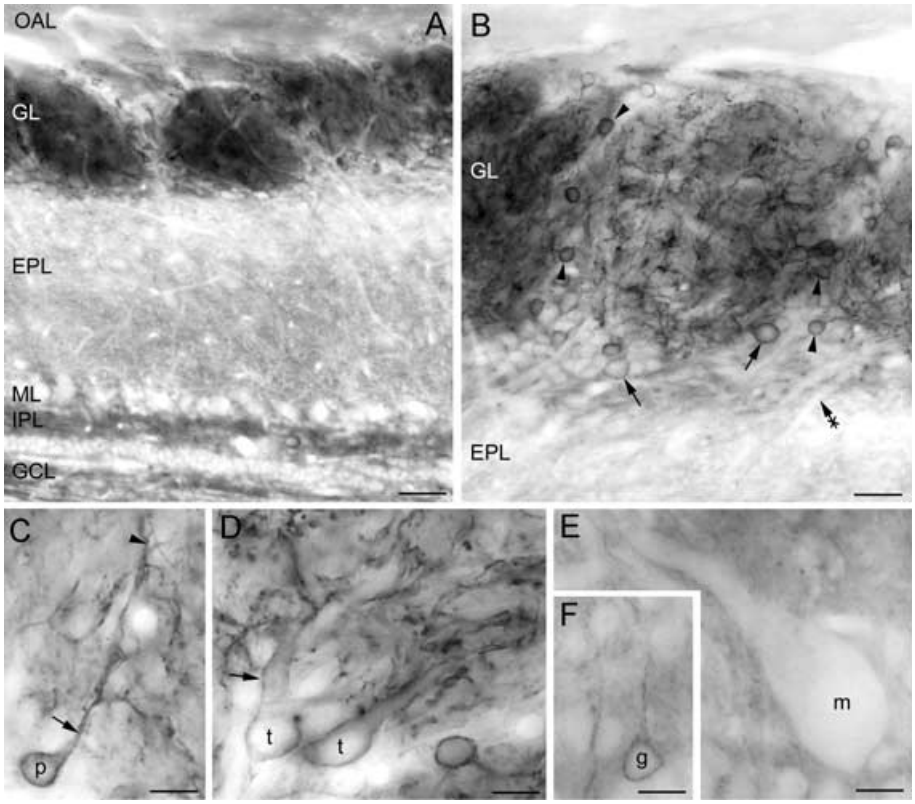

FIG. 1. Light microscopic demonstration of the distribution of immunoreactive HCN1 in the rat olfactory bulb. (A) The strongest labelling is detected in the glomerular layer (GL), followed by the internal plexiform layer (IPL), the granule cell layer (GCL) and the external plexiform layer (EPL). Olfactory axon bundles in the olfactory axon layer (OAL) are immunonegative. (B) Higher magnification of the GL demonstrates that the staining of the glomeruli originates from immunopositive juxtaglomerular cells (JGCs). Two subpopulations of HCN1-immunopositive JGCs are distinguished: small diameter, intensively labelled (e.g. arrowheads) and large diameter, weakly labelled (arrows) cells. Note the immunonegative mitral/tufted cell dendrites in the EPL (e.g. crossed arrow). (C) High magnification view of a small, intensively labelled JGC (p). The labelling intensity of the soma, proximal (arrow) and distal (arrowhead) dendrites is similar. (D) Somatic and proximal dendritic (arrow) membranes of two large diameter cells (t) are weakly immunoreactive. (E) An immunonegative mitral cell (m) is surrounded by diffuse neuropile labelling of the EPL. (F) An immunopositive granule cell (g) is shown in the GCL. ML, mitral cell layer. Scale bars: (A) 50 μm, (B) 25 μm and (C–F) 10 μm.

dendrites. In addition, a subpopulation of short-axon cells also showed HCN1 immunoreactivity in the granule cell layer, although the labelling mainly localized to the somatic and proximal dendritic cytoplasm rather than to the plasma membranes (data not shown).

In the glomerular layer, the SoMe and DeMe of a subset of JGC were labelled among many unlabelled neurons. Most of the HCN1-immunopositive cells were strongly labelled and were small (5–8 μm) in diameter (Fig. 1B). These cells typically had a thin, aspiny dendrite that branched in one glomerulus. The SoMe and proximal DeMe were labelled evenly, whereas their axons remained immunonegative (Fig. 1C). A few JGCs displayed lower levels of HCN1 immunoreactivity. These cells were larger in diameter (8–15 μm) and their thick apical dendrite branched mainly in one glomerulus (Fig. 1D) occasionally having thick lateral dendrites that ran in the outer third of the external plexiform layer. Higher magnifications revealed that the immunoreactivity of the dendrites and somata originated mainly from labelling of the plasma membrane. The axon initial segments of these cells were also immunopositive (not shown). Next, we estimated the proportion of the HCN1-immunopositive cells among the JGC population using the disector method (see Materials and methods). Consecutive semithin (0.5 μm thick) sections were cut from pre-embedding HCN1 immunoperoxidase-reacted sections (60 μm thick). The total number of neurons was assessed in toluidin blue-stained sections 2 μm apart from one another (glial cell bodies were not counted) and the HCN1-immunopositive cells were identified on consecutive, unstained sections. The percentage of HCN1-immunopositive cells was $11.8 \pm 0.3\%$ ($n = 3$ animals) of the total JGC population. The majority of the HCN1-immunopositive cells ($\approx 95\%$) were small in diameter and strongly immunopositive, indicating that the weakly HCN1-immunopositive population comprises less than 1% of the total JGCs.

It is known that JGCs are comprised of three major neuron populations, PGCs, short-axon cells and ETCs. Next, we carried out double-labelling experiments to determine which JGC population expresses HCN1. In the first series of experiments, we determined the immunoreactive GABA content of JGCs, including the HCN1-immunopositive populations. Consecutive semithin sections from pre-embedding HCN1 immunoperoxidase reactions were cut and either (i) stained for toluidin blue to identify neuronal somata (Fig. 2A), (ii) left unstained to identify HCN1-immunopositive somata (Fig. 2B) or (iii) immunoreacted for GABA to determine the GABA content of these nerve cells (Fig. 2C). Figure 3 shows the result of the quantitative analysis of the immunoreactive GABA content of JGCs in an adult rat. There are two distinct populations of JGCs according to the immunoreactive GABA content. The minority of the cells ($\approx 10\%$) is GABA immunonegative, whereas the rest of the JGCs were GABA immunopositive with variable levels of reactivity (also see Fig. 2C). Each strongly HCN1-immunopositive JGC had a detectable level of GABA immunoreactivity, suggesting that they are either PGCs or short-axon cells. As the strongly HCN1-positive cells always had a single dendrite

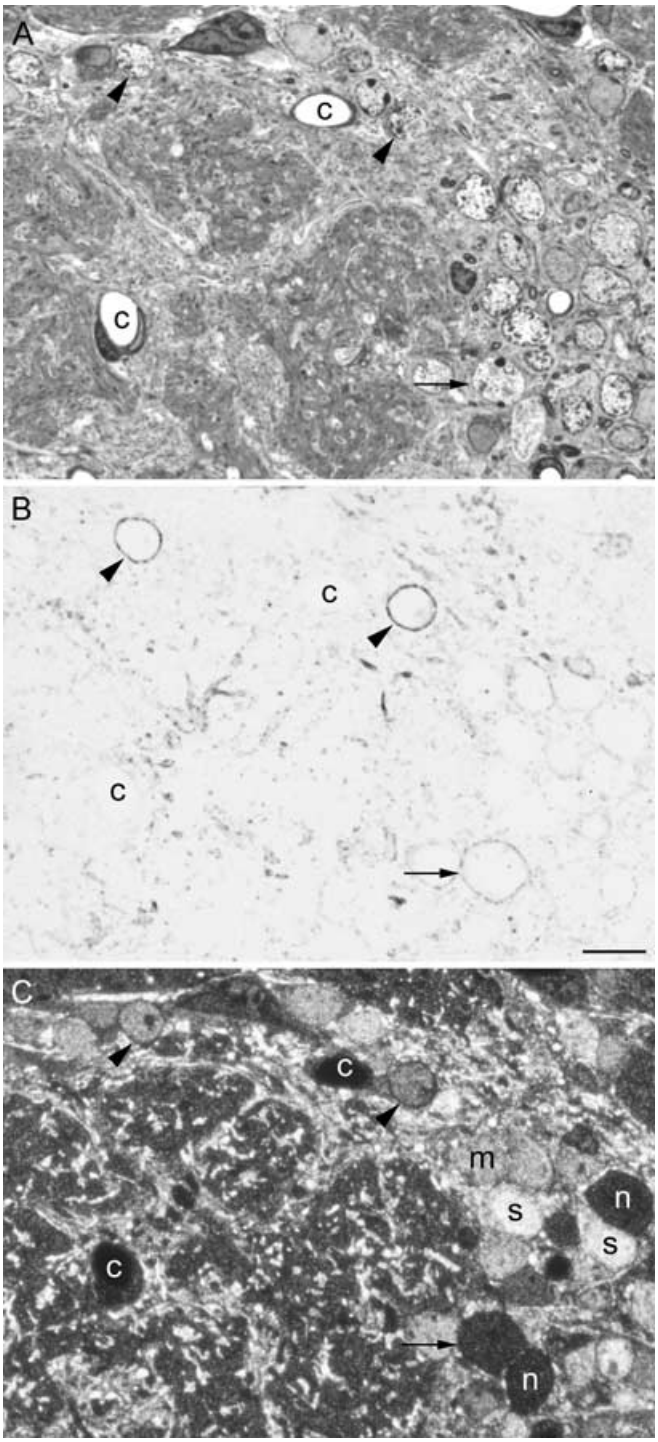

FIG. 2. HCN1-immunopositive juxtaglomerular cells show distinct levels of GABA immunoreactivity. (A–C) Serial semithin sections (0.5 µm thick) were stained for toluidin blue (A), HCN1 (B) and GABA (C). Two strongly HCN1-labelled cells (arrowheads) display moderate levels of GABA immunoreactivity. A large diameter, weakly HCN1-labelled cell (arrow) is immunonegative for GABA. Note the large variability in the levels of GABA immunoreactivity among periglomerular cells [e.g. strongly labelled cells (s), moderately labelled cells (arrowheads and m) and negative cells (arrow and n)]. c, capillaries. Scale bar: 10 µm.

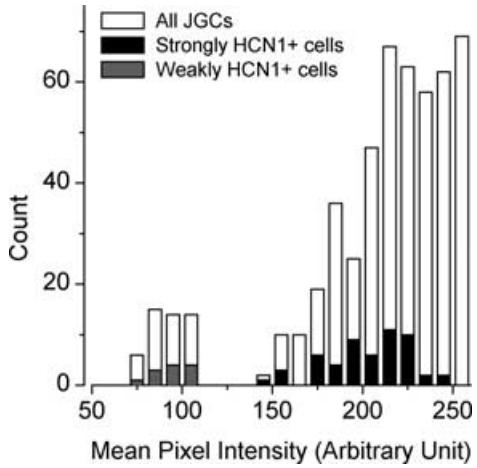

FIG. 3. Distribution of juxtaglomerular cells (JGCs) according to their immunoreactive GABA content. Immunoreactivity for GABA was revealed with an immunofluorescent method on semithin sections. Mean pixel intensity values (in arbitrary unit) were calculated for each cell and are plotted (unfilled/white columns). The histogram reveals two populations of JGCs according to their immunoreactive GABA content. The GABA-immunonegative population may correspond to the external tufted cells ($n = 49$ cells), whereas the GABA-immunopositive cells are the periglomerular cells ($n = 468$). All large diameter weakly HCN1-labelled cells (grey columns, $n = 12$) are GABA immunonegative (i.e. external tufted cells), whereas every strongly HCN1-positive cell (black-filled columns, $n = 54$) is GABA immunopositive (i.e. periglomerular cells).

entering a single glomerulus, and multiple dendritic processes leave the somata of short-axon cells (Pinching & Powell, 1971; Toida *et al.*, 1998), the strongly HCN1-positive cells are likely to be PGCs. All of the weakly HCN1-immunopositive JGCs fell into the GABA-immunonegative population. We repeated these experiments in two additional rats. In the second animal, the separation of the weakly and strongly HCN1-positive cells into GABA-negative and -positive populations, respectively, was identical to that described above. In the third rat, two of 12 weakly HCN1-positive cells were in the GABA-immunopositive population. The GABA immunonegativity of the large diameter, weakly HCN1-positive cells indicates that they are ETCs. To establish whether these cells are indeed glutamatergic, we carried out double immunofluorescent labelling for HCN1 and vGluT1 or vGluT2. All of the weakly HCN1-immunopositive large cells were immunopositive for vGluT2 (Fig. 4A and B), providing further evidence that they are glutamatergic ETCs. Not all vGluT2-immunopositive cells expressed detectable amounts of HCN1 (Fig. 4A and B) and none of the strongly HCN1-immunolabelled PGCs expressed either of the vGluTs.

Periglomerular cells can be further divided into subpopulations according to the content of the following neurochemical markers: TH, calbindin D28k or calretinin (Kosaka *et al.*, 1998). In order to determine whether the strongly HCN1-immunopositive cells comprise one of these PGC subpopulations, we carried out double immunofluorescent labelling for HCN1 and for the above-mentioned neurochemical markers. None of the strongly HCN1-immunopositive cells contained immunoreactive calretinin (0 of 271 HCN1-positive cells in four animals) or TH (0 of 263 HCN1-positive cells in three animals), whereas only a small fraction of them ($6.5 \pm 1.6\%$, 36 of 559 HCN1-positive cells in three rats) coexpressed calbindin D28k (Fig. 4C and D). These results indicate that the strongly HCN1-immunopositive cells comprise a novel PGC subpopulation.

Subcellular distribution of immunoreactive HCN1 in juxtaglomerular cells

The subcellular distribution of HCN1 in the MOB was studied using pre-embedding immunoperoxidase and immunogold techniques. In the glomerular layer, peroxidase reaction end-product covered the cytoplasm of some JGC somata and dendrites. Electron microscopic

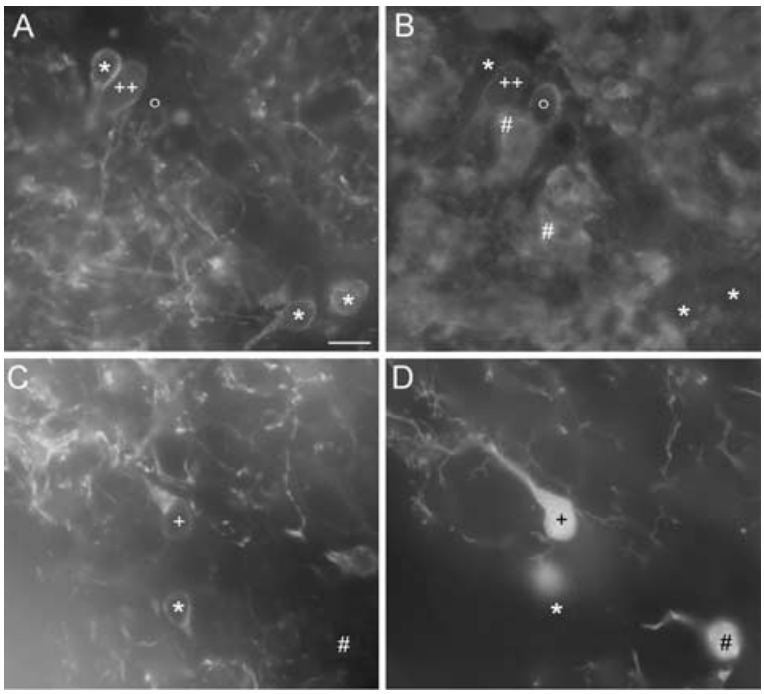

FIG. 4. Double immunofluorescent labelling for (A) HCN1, (B) vesicular glutamate transporter (vGluT)2, (C) HCN1 and (D) calbindin D-28k in the glomerular layer. (A and B) A weakly HCN1-immunopositive cell (++) expresses vGluT2. The strongly HCN1-immunopositive periglomerular cells (*) do not contain detectable levels of vGluT2. Note that not all vGluT2-immunopositive cells express HCN1 (o). Terminal zones of primary olfactory axons (#) are intensely labelled for vGluT2. (C and D) One of the strongly HCN1-immunopositive cells (+) expresses calbindin but another (*) is calbindin immunonegative. Not all calbindin-immunoreactive cells (#) show detectable levels of HCN1. Scale bar: 10 μm.

analysis of the immunogold reactions demonstrated that most of the gold particles for HCN1 were associated with the cytoplasmic side of SoMe or DeMe (Figs 5 and 6). These results are in agreement with the cytoplasmic location of the epitope(s) and also indicate that the majority of the immunosignal originates from plasma membrane labelling. No detectable staining was observed in glial processes or in primary olfactory axons and axon terminals.

In agreement with our light microscopic observations, we also detected three distinct levels of HCN1 immunoreactivity at the electron microscopic level in JGC SoMe. The plasma membranes of some small diameter cells were strongly outlined by gold particles (Fig. 5A), only a few cells were weakly labelled for HCN1 (Fig. 6B) and the majority of the cells had an undetectable level of HCN1 (Fig. 5A). The strongly HCN1-immunolabelled cell bodies had a large nucleus : cytoplasm ratio and a heterochromatic nucleus with few cytoplasmic organelles. In weakly labelled cells, the cytoplasm was large and the endoplasmic reticulum and Golgi apparatus were elaborate. These cells occasionally established somato-dendritic asymmetrical synaptic contacts and had a larger proportion of intracytoplasmic to plasma membrane immunoparticle number compared with that of strongly HCN1-labelled PGCs. Differences in the strength of immunoreactivity of dendritic processes were also apparent. Intensely labelled dendritic processes were typically found in the olfactory nerve-free zone (non-ON zone) of the glomeruli. These dendrites were usually small in diameter, received asymmetrical synapses from mitral/tufted cell dendrites (Fig. 5C) and occasionally established symmetrical synapses on other dendritic processes (Fig. 5B). A few strongly labelled dendrites received synapses from primary olfactory terminals inside the olfactory nerve termination zones (ON zone, e.g. Fig. 5D). All of these morphological features are consistent with PGCs being strongly HCN1 immunopositive. To directly demonstrate the presence of some of the molecular apparatus required for GABA release, we performed electron microscopic double immunolabelling for HCN1 and vesicular GABA transporter. As shown in Fig. 5B, vesicular GABA transporter-immunopositive vesicle clusters could be found in some of the strongly HCN1-immunopositive dendrites but never in weakly HCN1-positive dendrites. The weakly labelled dendrites were usually larger in diameter, often established asymmetrical dendro-dendritic synapses (Fig. 6D) and received asymmetrical synapses from primary olfactory axon terminals (Fig. 6E). These ultrastructural features are consistent with ETCs being moderately labelled for HCN1. We also tested whether these moderately labelled cells were immunopositive for vGluT1 or vGluT2. As illustrated in Fig. 6, electrondense 3′3-diaminobenzidine tetrahydrochloride (DAB) precipitates labelling vGluT2 were detected in large diameter, weakly HCN1-immunolabelled cell bodies and dendrites.

Immunoparticles labelling HCN1 appeared randomly distributed along the DeMe and SoMe, without detectable association with pre- or post-synaptic membranes of symmetrical or asymmetrical synapses. Using the pre-embedding immunogold method, however, the lack of synaptic enrichment of a transmembrane protein cannot be concluded from the lack of synaptic immunolabelling (Nusser *et al.*, 1995). Unfortunately, we were unable to reveal the subcellular distribution of HCN1 with a post-embedding technique with the currently available antibodies. Thus, it remains to be determined whether HCN1 is enriched in synaptic junctions or is present exclusively extrasynaptically in JGCs.

Quantitative analysis of HCN1 immunogold labelling in juxtaglomerular cells

To determine the differences in the immunogold densities between strongly labelled PGCs and weakly labelled ETCs, and to establish possible differences in HCN1 density in distinct subcellular compartments,

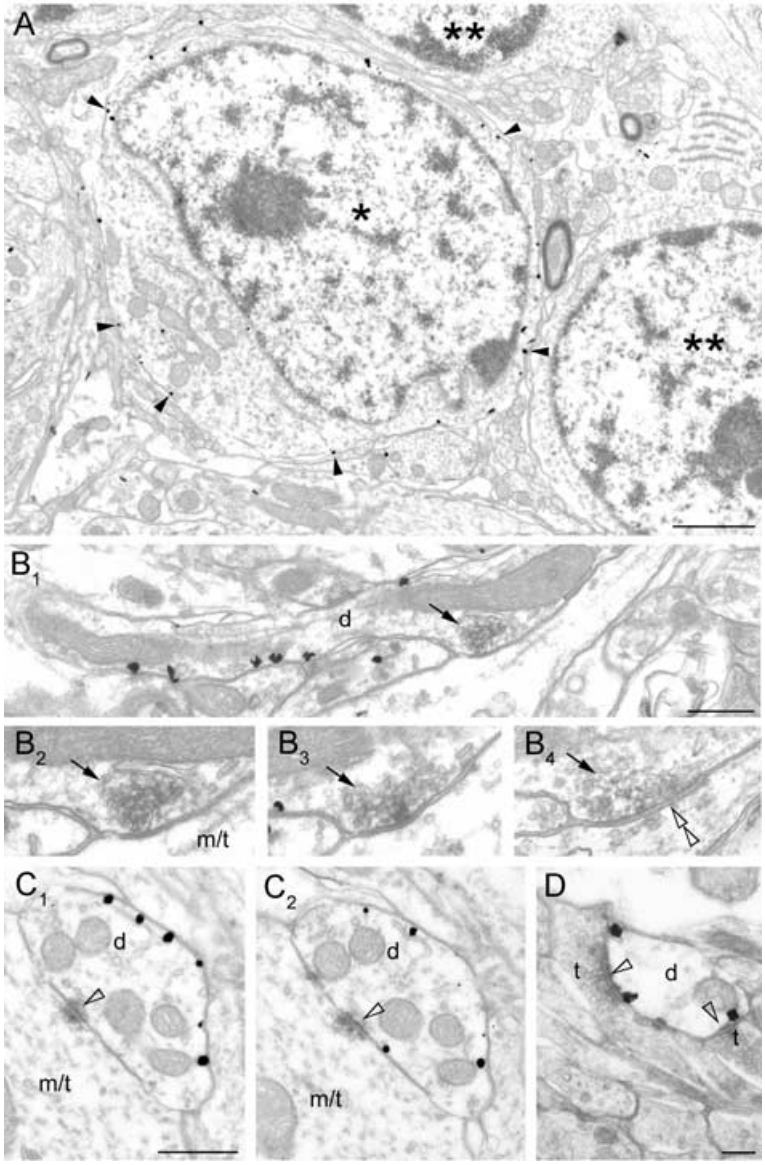

FIG. 5. Electron microscopic immunogold labelling for HCN1 in the glomerular layer. (A) Most immunogold particles labelling HCN1 (e.g. arrowheads) are found along the somatic plasma membrane of a periglomerular cell (*). This strongly labelled cell is surrounded by two immunonegative periglomerular cells (**). (B_{1-4}) Electron micrographs showing double immunolabelling reactions for HCN1 (immunogold reaction) and vesicular GABA transporter (VGAT) (DAB reaction). (B_1) A VGAT-immunopositive vesicle cluster (arrow) is present in the cytoplasm of a strongly HCN1-immunolabelled dendrite (d). B_{2-4} demonstrate in serial sections that the same dendrite establishes a symmetrical synapse (double open arrowhead) with a presumed mitral/tufted cell dendrite (m/t). (C_{1-2}) Serial electron microscopic sections of an intensively HCN1-labelled dendrite (d). This dendrite receives an asymmetrical synapse (open arrowhead) from a presumed mitral/tufted cell dendrite (m/t). (D) Primary olfactory axon terminals (t) establish asymmetrical synapses (open arrowheads) on an HCN1-immunopositive small diameter dendrite (d). Scale bars: (A) 1 μm; (B and C) 0.5 μm and (D) 0.2 μm.

the immunogold reactions were quantitatively analysed in the glomerular layer. We determined the immunogold densities in the following plasma membrane compartments: SoMe of immunopositive ETCs, SoMe of immunopositive PGCs, DeMe of mitral/tufted cells and DeMe of unidentified immunopositive neurons. The density of HCN1 immunogold labelling was significantly higher ($P < 0.001$, unpaired *t*-test) in all of these compartments (ETC SoMe, 5.9 ± 0.9 particle/μm^2, $n = 11$; mitral/tufted cell DeMe, 8.2 ± 2.1 particle/μm^2, $n = 11$ and PGC SoMe, 20.7 ± 1.8 particle/μm^2, $n = 9$) than the non-specific labelling density as determined over the nuclei of JGCs (0.1 ± 0.02 particle/μm^2, $n = 25$). Following the subtraction of non-specific labelling, the calculated immunogold density for HCN1 was ≈3.5 times higher ($P < 0.001$, unpaired *t*-test) in the SoMe of immunopositive PGCs (0.95 ± 0.08 particle/μm) than in the SoMe of ETCs (0.27 ± 0.04 particle/μm). We repeated these experiments in a second animal and found virtually the same result. The difference (5.1-fold) in immunogold densities between PGC (1.07 ± 0.06 particle/μm) and ETC (0.21 ± 0.02 particle/μm) SoMe was highly significant ($P < 0.001$).

Next, we aimed to determine whether the DeMe of ETCs contained significantly higher HCN1 density than somatic membranes, as in cortical and hippocampal pyramidal cells (Lorincz *et al.*, 2002). In Fig. 7, the distributions of immunoparticle densities are plotted for all immunopositive dendrites and superimposed are the SoMe compartments. Of 111 immunolabelled dendrites, we could positively identify 11 dendrites as belonging to mitral/tufted cells

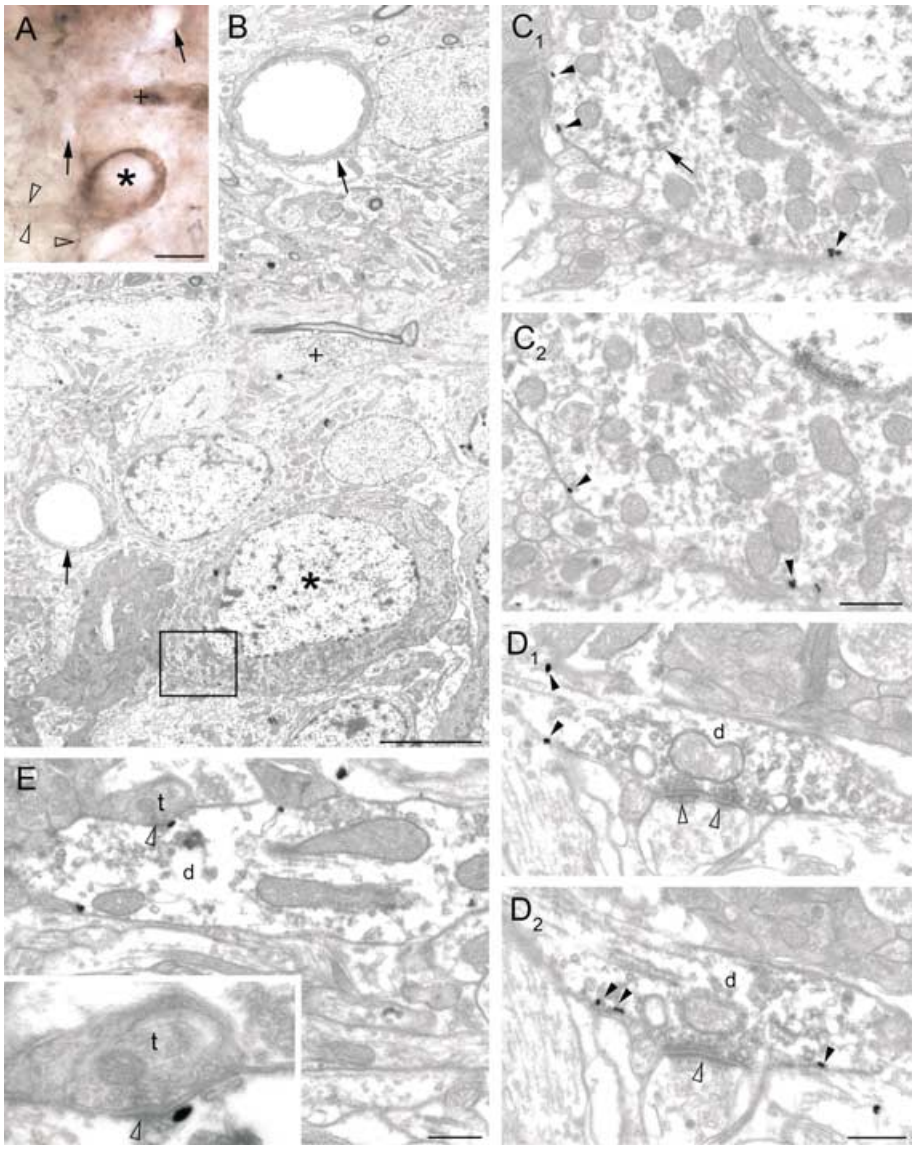

FIG. 6. Subcellular distribution of HCN1 in vesicular glutamate transporter (vGluT)2-immunopositive external tufted cells (ETCs). (A and B) Light and electron micrographs showing the same region of the glomerular layer. Arrows point to two capillaries. (A) Brown 3′3-diaminobenzidine tetrahydrochloride (DAB) precipitate, indicating vGluT2 immunoreactivity, is visible in the cytoplasm of a double-labelled ETC (*). The immunogold labelling is apparent in the proximal dendrites (open arrowheads) of the same cell. A strongly vGluT2-labelled dendrite is indicated by +. (B) Electron-dense DAB precipitate is clearly visible in the cytoplasm of the double-labelled ETC (*). Boxed area is shown at higher magnification in (C). (C_{1-2}) A few immunogold particles (arrowheads) labelling HCN1 are found along the somatic plasma membrane. Electron-dense DAB precipitate is present in the cytoplasm (arrow). (C_1 and C_2) Serial sections. (D_{1-2}) Consecutive sections of a weakly HCN1-immunopositive (arrowheads) dendrite (d) that establishes an asymmetrical synapse (open arrowheads) with an immunonegative dendrite. The synaptic vesicles are covered with DAB precipitate indicating the presence of vGluT2. (E) A double immunopositive ETC dendrite (d) receives an asymmetrical synapse (open arrowhead) from a primary olfactory axon terminal (t). The synapse is enlarged in the insert. Scale bars: (A) 10 μm, (B) 5 μm and (C–E) 0.5 μm.

(large relatively empty profiles, establishing asymmetrical synapses) and the immunoparticle density for HCN1 was not significantly different ($P = 0.33$, unpaired *t*-test) in these DeMe (0.38 ± 0.09 particle/μm) to that in the SoMe of ETCs (0.27 ± 0.04 particle/μm). In a second animal, we also found no significant difference ($P = 0.27$) in HCN1 densities between these two plasma membrane compartments (ETC SoMe, 0.21 ± 0.02 particle/μm and mitral/tufted DeMe, 0.27 ± 0.06 particle/μm). The possibility that some mitral cell apical dendrites contribute to the weakly HCN1-immunopositive dendritic population in the glomeruli cannot be excluded. However, for the following reasons, we believe that it is very unlikely. First, only a small fraction of the mitral/tufted cell dendrites is labelled in the glomeruli. The ETCs that are immunopositive for HCN1 at the somatic level form a small subpopulation of all mitral and tufted cells. This is consistent with the small proportion of HCN1-labelled mitral/tufted-like dendrites in the glomerular layer. If some mitral cell distal dendrites were labelled for HCN1, this would require a heterogeneity in the mitral cell population according to their HCN1 expression. The colocalization of HCN1 and vGluT2 is demonstrated in some weakly HCN1-positive mitral/tufted dendrites (Fig. 6). Under our conditions, mitral cells do not express this form of vesicular glutamate transporter but they are vGluT1 immunopositive (N.B.H and Z.N. unpublished observation). However, as shown in Fig. 4, the somata of several ETCs are vGluT2 immunopositive, some of which contain HCN1. These results demonstrate that the distance-dependent difference in HCN1 density on the somato-dendritic surface of

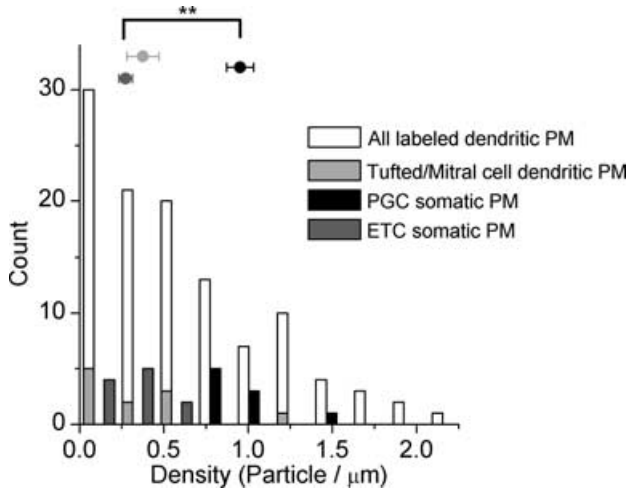

FIG. 7. Quantitative evaluation of HCN1 immunogold labelling in the glomerular layer of a rat olfactory bulb. Membrane-associated immunogold particles were counted and their densities calculated (see Materials and methods). Only immunolabelled profiles are included in the analysis (all labelled dendrites; white/unfilled columns, $n = 111$ dendrites). The immunoparticle density for HCN1 is significantly lower ($^{**}P < 0.001$, unpaired *t*-test) in somatic plasma membranes (PMs) of external tufted cells (ETCs) (dark grey columns; mean ±SEM marked with dark grey-filled circle, $n = 11$ cells) than in labelled periglomerular cells (PGCs) (black-filled columns; mean ±SEM marked with black-filled circle, $n = 9$ cells). No significant difference is detected between the tufted cell somatic and mitral/tufted cell dendritic (light grey columns; average ±SEM marked with light grey-filled circle, $n = 11$ dendrites) immunogold densities. Note that the immunogold density of the most intensively labelled dendrites is only twice as large as the mean density of PGC somatic PMs.

pyramidal cells (Lorincz *et al.*, 2002) is not a general feature of the subcellular distribution of HCN1.

Discussion

Our results reveal a cell type-specific expression of HCN1 in the MOB. Most of the projecting neurons of the MOB, the mitral, internal- and middle-tufted cells, do not express detectable levels of HCN1. Moderate staining of the granule cell layer and external plexiform layer originates from weakly labelled granule cell dendrites. Three distinct subpopulations of the JGCs can be distinguished according to their HCN1 immunoreactivity. Approximately 10% of JGCs contain a high density of HCN1. These cells are small in diameter and are GABA and vesicular GABA transporter immunopositive, comprising a subpopulation of PGCs. Some GABA-immunonegative and vGluT2-immunopositive ETCs (<1% of all JGCs) express lower levels of HCN1. The rest of the JGCs are immunonegative for HCN1. Quantitative electron microscopic immunogold localizations revealed that the SoMe of PGCs has approximately four times more immunoreactive HCN1 than that of ETCs. Unlike in hippocampal and neocortical pyramidal cells, immunogold densities for HCN1 do not significantly differ in SoMe and DeMe of ETCs.

Heterogeneity of juxtaglomerular cells

Juxtaglomerular cells of the MOB have been extensively studied using neuroanatomical and electrophysiological techniques. Several subpopulations have been distinguished according to the axo-dendritic arborizations, synaptic input–output relationships and neurotransmitter/neurochemical content (Pinching & Powell, 1971; Kosaka *et al.*, 1998; Toida *et al.*, 1998). For example, JGCs can be divided into three subpopulations based on their axo-dendritic arborizations: ETCs, PGCs and short axon cells. Based on their neurochemical contents, JGCs have been subdivided into TH-, calretinin- and calbindin-immunopositive subpopulations. According to the synaptic input–output relationships, JGCs have been divided into two subgroups: type I cells, receiving strong excitation from ON terminals in the ON zone and type II cells, with dendritic arbors mainly restricted to the non-ON zone (Kosaka *et al.*, 1998). The firing and passive membrane properties of these cells have also been used to generate subcategories (McQuiston & Katz, 2001). In the present study, we also found that the JGCs are heterogeneous according to their HCN1 content. A subset of GABA-immunopositive PGCs expresses a high density of HCN1, some ETCs have intermediate HCN1 densities and the majority of JGCs are immunonegative for HCN1. We performed series of double-labelling experiments to correlate the HCN1-immunopositive cell populations with those previously described, but they did not correspond to either of the PGC subpopulations. All strongly HCN1-immunopositive PGCs were immunonegative for TH and calretinin and only a small fraction of them contained immunoreactive calbindin, indicating that they represent a new subpopulation of PGCs. Although only 6% of these cells contained calbindin, their synaptic input–output relationships resembled those of calbindin-immunopositive cells (Toida *et al.*, 1998). They received only few asymmetrical synapses from ON terminals and mainly established symmetrical dendro-dendritic synaptic contacts with mitral/tufted cell dendrites in the non-ON zone of the glomerulus. In contrast to the TH-immunopositive cells (Toida *et al.*, 2000), they did not seem to form reciprocal synapses with the mitral/tufted cell dendrites. These results indicate an even larger heterogeneity of JGCs than previously recognized and raise the question of whether JGCs can indeed be subdivided into morphologically and functionally well-defined, non-overlapping subpopulations or whether they form a heterogeneous cell class with regard to their molecular content, axo-dendritic arborizations, synaptic input–output relationships and active and passive membrane properties.

Cell surface distribution of HCN1

In the last decade or so, the cell surface distribution of ligand-gated ion channels has been extensively studied using high-resolution localization techniques (Mohler *et al.*, 1997; Ottersen & Landsend, 1997; Petralia *et al.*, 1998; Somogyi *et al.*, 1998; Conti & Weinberg, 1999; Nusser, 2000; Craig & Boudin, 2001). This approach revealed, for example, complex and highly regulated subcellular distributions of GABA and glutamate receptors and provided vital information about how inhibitory and excitatory synapses operate in the CNS. Similarly, for voltage-gated ion channels, their precise location and density in specific subcellular compartments will also play a critical role in determining the functional consequences of their activation (Yuste & Tank, 1996; Magee, 2003). To date, very few studies have applied quantitative, high-resolution localization techniques to determine the cell surface distribution of voltage-gated ion channels. First, Hu *et al.* (2001) used electron microscopic immunogold localization to demonstrate that the large-conductance voltage- and Ca-activated K channel is concentrated in pre-synaptic active zones of glutamatergic axon terminals but is absent from post-synaptic dendritic membranes. Lorincz *et al.* (2002) studied the subcellular distribution of HCN1 in neocortical and hippocampal pyramidal cells and found that the density of this subunit in pyramidal cell apical dendrites increases as a function of distance from the soma. Furthermore, they also showed that the subcellular compartment also influences the channel density, because dendritic spines had a significantly lower HCN1 density than shafts at the same distance from the soma. In the present study, we revealed three distinct levels of HCN1 densities in the SoMe of JGCs: strongly HCN1-immunopositive PGCs had approximately four times higher immunogold densities in their SoMe than those of

immunolabelled ETCs and the majority (≈90%) of the JGCs had undetectable levels of HCN1. Furthermore, we could not detect significant differences in the densities of HCN1 between SoMe and DeMe of ETCs. This result is in sharp contrast to that found in cortical pyramidal cells and establishes that the distance-dependent increase in HCN1 density is not a general feature of HCN1 expression but is a specialization seen in some nerve cells but not in others. Our results clarify cell type-specific rules governing the subcellular distribution of HCN1 and highlight potential problems that could arise from over-simplified generalizations.

Functional predictions from the cellular and subcellular distributions of HCN1 in juxtaglomerular cells

One of the most fundamental roles of I_h is its involvement in the generation of rhythmic activities in the heart and in several brain regions (Pape, 1996). Rhythmic activities at varying frequencies are prominent in the MOB and they may be essential for sensory information coding and olfactory discrimination (Laurent, 2002). The cellular and molecular mechanisms underlying olfactory oscillations have been extensively studied, but almost nothing is known about the role of I_h in the generation of oscillations at different frequencies. Our results predict the differential involvement of distinct PGCs in olfactory oscillations. Based on the activation kinetics of I_h formed from HCN1 subunits (Chen *et al.*, 2001; Ishii *et al.*, 2001; Ulens & Tytgat, 2001), we suggest that some JGCs will possess sub- or suprathreshold oscillations in the theta frequency range. As they provide GABAergic input to the apical tuft of mitral cells, rhythmic $GABA_A$ receptor-mediated inhibition is predicted to interact with and structure the incoming excitatory inputs from primary olfactory axons. This local temporal structuring of the excitatory drive to mitral cells will have a profound influence on the timing of action potential firing of these cells. A subpopulation of spontaneously oscillating and bursting neurons has been described in JGCs beside standard firing cells (McQuiston & Katz, 2001). These cells possess calcium-channel-dependent low-threshold spikes. Neurons that produced these low-threshold spikes fell into two morphological categories, some had characteristics typical of ETCs but the majority were periglomerular inhibitory neurons (McQuiston & Katz, 2001). Although these interneurons had mostly spiny dendrites in contrast to the HCN1-immunopositive cells, it will be interesting to correlate the *in vitro* firing behaviours and the HCN subunit expression of JGCs. In a recent study, Cadetti & Belluzzi (2001) used patch-clamp recordings from *in vitro* slices to investigate I_h in JGCs. This study showed that I_h is present in all JGCs and that tonically active I_h plays a role in setting the resting membrane potential. Furthermore, experimentally induced low frequency oscillations in JGCs were reduced in the presence of I_h blockers. At first glance, these results are at odds with our immunolocalization of HCN1 in the MOB, showing that only 10% of the JGCs express detectable levels of HCN1. Two possibilities may explain this discrepancy. First, functional HCN1 channels may be present in the remaining 90% of the JGCs at a low density, undetectable with our immunolocalization techniques. A more likely explanation is that other HCN subunits are expressed in these cells. Indeed, studies using *in situ* hybridization techniques revealed that all HCN subunits, although with different patterns and intensities, are expressed in the MOB (Santoro *et al.*, 1998; Moosmang *et al.*, 1999). Should distinct JGCs express different HCN subunits, a large variability in the activation kinetics of I_h is predicted among JGCs. Furthermore, because of the distinct activation and deactivation kinetics of I_h, we would envisage a differential involvement of distinct JGCs in network oscillations of different frequencies. The molecular identification of *in vivo* recorded and identified JGCs will be necessary to test this prediction experimentally.

A hyperpolarization-activated current has also been found in pre-synaptic calyciform axon terminals making synapses on chick ciliary ganglion neurons (Fletcher & Chiappinelli, 1992), calyx of Held in the medial nucleus of the trapezoid body of the rat (Cuttle *et al.*, 2001) and in rat cerebellar basket cell axons (Southan *et al.*, 2000), where it regulates the release of GABA. Beaumont *et al.* (2002) have recently reported that I_h contributes to the induction of long-term facilitation of synaptic transmission following intense pre-synaptic activity at crayfish neuromuscular junctions. As PGCs and ETCs also release transmitter from their dendrites, the dendritic HCN1/I_h could also serve as a 'pre-synaptic' ion channel to regulate the release of GABA or glutamate, respectively, in an activity-dependent manner. Alternatively, although long-term plasticity at these synapses has not been described to our knowledge, I_h-dependent long-term changes in synaptic strength may also be operational. These predictions could be tested experimentally using paired intracellular recordings.

Another important role of I_h has been revealed in hippocampal and neocortical pyramidal cells (Magee, 1998, 1999; Williams & Stuart, 2000). In these cells, I_h was shown to be responsible for the location independence of the temporal summation of excitatory post-synaptic potentials (EPSPs). For example, in CA1 pyramidal cells under control conditions, distally generated EPSPs, when evoked with short trains of high frequency stimuli, showed a pattern of summation similar to that of their proximally terminating counterparts. However, the distance dependence of temporal summation, as predicted from passive cable theory, was revealed in the presence of specific I_h blockers. Depolarizing EPSPs deactivate I_h which results in the speeding of EPSP decay times. As the density of I_h in pyramidal cell dendrites increases as a function of distance from the soma, the more distally evoked EPSPs will have a faster decay at the site of generation (Magee, 1998, 1999). Unlike in cortical pyramidal cells, we have found that the immunogold density for HCN1 did not significantly differ in the SoMe and DeMe of ETCs. External tufted cells also differ from pyramidal cells in that the majority of their excitatory inputs arise from a single source, the ON terminals. Thus, a graded density of HCN1 would not be required to fulfil the same role in ETCs as described in pyramidal cells. However, the moderate density of HCN1 in these cells predicts that the decay of the ON-evoked EPSPs will be substantially shortened, making the cells more susceptible to the precise temporal coincidence of the incoming synaptic inputs to achieve significant summation. It will be interesting to test the effect of I_h blockers on the kinetics of ON-evoked EPSPs and on the temporal precision of the output of the moderately HCN1-positive ETCs and to compare it with those cells (e.g. inner and middle tufted and mitral cells) which have undetectable HCN1 expression.

Acknowledgements

Funds from the Hungarian Science Foundation (T 32329), the Howard Hughes Medical Institute, the Wellcome Trust, the Boehringer Ingelheim Fond and the Japan Science and Technology Corporation are gratefully acknowledged. We would like to thank Drs Mark Farrant and Attila Losonczy for their comments on the manuscript and Dr Peter Somogyi for the antibody to GABA.

Abbreviations

DAB, 3′3-diaminobenzidine tetrahydrochloride; DeMe, dendritic plasma membrane; EPSP, excitatory post-synaptic potential; ETC, external tufted cell; HCN, hyperpolarization-activated and cyclic nucleotide-gated channel; I_h, hyperpolarization-activated cationic current; JGC, juxtaglomerular cell; MOB, main olfactory bulb; NGS, normal goat serum; ON, olfactory nerve; PGC, periglomerular cell; SoMe, somatic plasma membrane; TBS, Tris-buffered saline; TH, tyrosine hydroxylase; vGluT, vesicular glutamate transporter.

References

Accili, E.A., Proenza, C., Baruscotti, M. & DiFrancesco, D. (2002) From funny current to HCN channels: 20 years of excitation. *News Physiol. Sci.*, **17**, 32–37.

Adrian, E.D. (1942) Olfactory reactions in the brain of the hedgehog. *J. Physiol. (Lond.)*, **100**, 459–473.

Adrian, E.D. (1950) The electrical activity of the mammalian olfactory bulb. *Electroenc. Clin. Neurophys.*, **2**, 377–388.

Beaumont, V., Zhong, N., Froemke, R.C., Ball, R.W. & Zucker, R.S. (2002) Temporal synaptic tagging by I_h activation and actin. Involvement in long-term facilitation and cAMP-induced synaptic enhancement. *Neuron*, **33**, 601–613.

Berger, T., Larkum, M.E. & Luscher, H.R. (2001) High I_h channel density in the distal apical dendrite of layer V pyramidal cells increases bidirectional attenuation of EPSPs. *J. Neurophysiol.*, **85**, 855–868.

Buzsaki, G. (2002) Theta oscillations in the hippocampus. *Neuron*, **33**, 325–340.

Cadetti, L. & Belluzzi, O. (2001) Hyperpolarisation-activated current in glomerular cells of the rat olfactory bulb. *Neuroreport*, **12**, 3117–3120.

Chen, S., Wang, J. & Siegelbaum, S.A. (2001) Properties of hyperpolarization-activated pacemaker current defined by coassembly of HCN1 and HCN2 subunits and basal modulation by cyclic nucleotide. *J. Gen. Physiol.*, **117**, 491–504.

Conti, F. & Weinberg, R.J. (1999) Shaping excitation at glutamatergic synapses. *Trends Neurosci.*, **22**, 451–458.

Craig, A.M. & Boudin, H. (2001) Molecular heterogeneity of central synapses: afferent and target regulation. *Nature Neurosci.*, **4**, 569–578.

Cuttle, M.F., Rusznak, Z., Wong, A.Y., Owens, S. & Forsythe, I.D. (2001) Modulation of a presynaptic hyperpolarization-activated cationic current (I_h) at an excitatory synaptic terminal in the rat auditory brainstem. *J. Physiol. (Lond.)*, **534**, 733–744.

Fletcher, G.H. & Chiappinelli, V.A. (1992) An inward rectifier is present in presynaptic nerve terminals in the chick ciliary ganglion. *Brain Res.*, **575**, 103–112.

Freeman, W.J. (1975) *Mass Action in the Nervous System*. Academic Press, New York.

Freeman, W.J. (1976) *Quantitative Patterns of Integrated Neural Activity.* Sinauer and Assoc, Sunderland, MA.

Gauss, R., Seifert, R. & Kaupp, U.B. (1998) Molecular identification of a hyperpolarization-activated channel in sea urchin sperm. *Nature*, **393**, 583–587.

Gundersen, H.J.G. (1977) Notes on the estimation of the numerical density of arbitrary particles: the edge effect. *J. Microsc.*, **111**, 219–223.

Hu, H., Shao, L.R., Chavoshy, S., Gu, N., Trieb, M., Behrens, R., Laake, P., Pongs, O., Knaus, H.G., Ottersen, O.P. & Storm, J.F. (2001) Presynaptic Ca^{2+}-activated K^+ channels in glutamatergic hippocampal terminals and their role in spike repolarization and regulation of transmitter release. *J. Neurosci.*, **21**, 9585–9597.

Ishii, T.M., Takano, M. & Ohmori, H. (2001) Determinants of activation kinetics in mammalian hyperpolarization-activated cation channels. *J. Physiol. (Lond.)*, **537**, 93–100.

Kosaka, K., Toida, K., Aika, Y. & Kosaka, T. (1998) How simple is the organization of the olfactory glomerulus?: the heterogeneity of so-called periglomerular cells. *Neurosci. Res.*, **30**, 101–110.

Laurent, G. (2002) Olfactory network dynamics and the coding of multidimensional signals. *Nature Rev. Neurosci.*, **3**, 884–895.

Laurent, G. & Davidowitz, H. (1994) Encoding of olfactory information with oscillating neural assemblies. *Science*, **265**, 1872–1875.

Lorincz, A., Notomi, T., Tamas, G., Shigemoto, R. & Nusser, Z. (2002) Polarized and compartment-dependent distribution of HCN1 in pyramidal cell dendrites. *Nature Neurosci.*, **5**, 1185–1193.

Ludwig, A., Zong, X., Jeglitsch, M., Hofmann, F. & Biel, M. (1998) A family of hyperpolarization-activated mammalian cation channels. *Nature*, **393**, 587–591.

Magee, J.C. (1998) Dendritic hyperpolarization-activated currents modify the integrative properties of hippocampal CA1 pyramidal neurons. *J. Neurosci.*, **18**, 7613–7624.

Magee, J.C. (1999) Dendritic I_h normalizes temporal summation in hippocampal CA1 neurons. *Nature Neurosci.*, **2**, 508–514.

Magee, J.C. (2000) Dendritic integration of excitatory synaptic input. *Nature Rev. Neurosci.*, **1**, 181–190.

Magee, J.C. (2003) A prominent role for intrinsic neuronal properties in temporal coding. *Trends Eurosci.*, **26**, 14–16.

McQuiston, A.R. & Katz, L.C. (2001) Electrophysiology of interneurons in the glomerular layer of the rat olfactory bulb. *J. Neurophysiol.*, **86**, 1899–1907.

Mohler, H., Benke, D., Benson, J., Luscher, B., Rudolph, U. & Fritschy, J.M. (1997) *Diversity in Structure, Pharmacology, and Regulation of $GABA_A$ Receptors*. Humana Press, Totowa, NJ.

Monteggia, L.M., Eisch, A.J., Tang, M.D., Kaczmarek, L.K. & Nestler, E.J. (2000) Cloning and localization of the hyperpolarization-activated cyclic nucleotide-gated channel family in rat brain. *Brain Res. Mol. Brain Res.*, **81**, 129–139.

Moosmang, S., Biel, M., Hofmann, F. & Ludwig, A. (1999) Differential distribution of four hyperpolarization-activated cation channels in mouse brain. *Biol. Chem.*, **380**, 975–980.

Moosmang, S., Stieber, J., Zong, X., Biel, M., Hofmann, F. & Ludwig, A. (2001) Cellular expression and functional characterization of four hyperpolarization-activated pacemaker channels in cardiac and neuronal tissues. *Eur. J. Biochem.*, **268**, 1646–1652.

Nusser, Z. (2000) AMPA and NMDA receptors: similarities and differences in their synaptic distribution. *Curr. Opin. Neurobiol.*, **10**, 337–341.

Nusser, Z., Roberts, J.D.B., Baude, A., Richards, J.G., Sieghart, W. & Somogyi, P. (1995) Immunocytochemical localization of the a1 and b2/3 subunits of the $GABA_A$ receptor in relation to specific GABAergic synapses in the dentate gyrus. *Eur. J. Neurosci.*, **7**, 630–646.

Ottersen, O.P. & Landsend, A.S. (1997) Organization of glutamate receptors at the synapse. *Eur. J. Neurosci.*, **9**, 2219–2224.

Pape, H.C. (1996) Queer current and pacemaker: the hyperpolarization-activated cation current in neurons. *Annu. Rev. Physiol.*, **58**, 299–327.

Pape, H.C. & McCormick, D.A. (1989) Noradrenaline and serotonin selectively modulate thalamic burst firing by enhancing a hyperpolarization-activated cation current. *Nature*, **340**, 715–718.

Petralia, R.S., Rubio, M.E. & Wenthold, R.J. (1998) Selectivity in the distribution of glutamate receptors in neurons. *Cell Biol. Int.*, **22**, 603–608.

Pinching, A.J. & Powell, T.P. (1971) The neuron types of the glomerular layer of the olfactory bulb. *J. Cell Sci.*, **9**, 305–345.

Santoro, B., Grant, S.G., Bartsch, D. & Kandel, E.R. (1997) Interactive cloning with the SH3 domain of N-src identifies a new brain specific ion channel protein, with homology to eag and cyclic nucleotide-gated channels. *Proc. Natl Acad. Sci. U.S.A.*, **94**, 14 815–14 820.

Santoro, B., Liu, D.T., Yao, H., Bartsch, D., Kandel, E.R., Siegelbaum, S.A. & Tibbs, G.R. (1998) Identification of a gene encoding a hyperpolarization-activated pacemaker channel of brain. *Cell*, **93**, 717–729.

Schwindt, P.C. & Crill, W.E. (1997) Modification of current transmitted from apical dendrite to soma by blockade of voltage- and Ca^{2+}-dependent conductances in rat neocortical pyramidal neurons. *J. Neurophysiol.*, **78**, 187–198.

Singer, W. (1999) Neuronal synchrony: a versatile code for the definition of relations? *Neuron*, **24**, 49–65.

Sloviter, R.S., Ali-Akbarian, L., Horvath, K.D. & Menkens, K.A. (2001) Substance P receptor expression by inhibitory interneurons of the rat hippocampus: enhanced detection using improved immunocytochemical methods for the preservation and colocalization of GABA and other neuronal markers. *J. Comp. Neurol.*, **430**, 283–305.

Somogyi, P., Hodgson, A.J., Chubb, I.W., Penke, B. & Erdei, A. (1985) Antisera to g-aminobutyric acid. II. Immunocytochemical application to the central nervous system. *J. Histochem. Cytochem.*, **33**, 240–248.

Somogyi, P., Nusser, Z., Roberts, J.D.B. & Lujan, R. (1998) *Precision and Variability in the Placement of Pre- and Postsynaptic Receptors in Relation to Neurotransmitter Release Sites*. HFSP, Strasbourg.

Southan, A.P., Morris, N.P., Stephens, G.J. & Robertson, B. (2000) Hyperpolarization-activated currents in presynaptic terminals of mouse cerebellar basket cells. *J. Physiol. (Lond.)*, **526**, 91–97.

Stuart, G. & Spruston, N. (1998) Determinants of voltage attenuation in neocortical pyramidal neuron dendrites. *J. Neurosci.*, **18**, 3501–3510.

Toida, K., Kosaka, K., Heizmann, C.W. & Kosaka, T. (1998) Chemically defined neuron groups and their subpopulations in the glomerular layer of the rat main olfactory bulb. III. Structural features of calbindin D28K-immunoreactive neurons. *J. Comp. Neurol.*, **392**, 179–198.

Toida, K., Kosaka, K., Aika, Y. & Kosaka, T. (2000) Chemically defined neuron groups and their subpopulations in the glomerular layer of the rat main olfactory bulb. IV. Intraglomerular synapses of tyrosine hydroxylase-immunoreactive neurons. *Neuroscience*, **101**, 11–17.

Ulens, C. & Tytgat, J. (2001) Functional heteromerization of HCN1 and HCN2 pacemaker channels. *J. Biol. Chem.*, **276**, 6069–6072.

Williams, S.R. & Stuart, G.J. (2000) Site independence of EPSP time course is mediated by dendritic I_h in neocortical pyramidal neurons. *J. Neurophysiol.*, **83**, 3177–3182.

Yuste, R. & Tank, D.W. (1996) Dendritic integration in mammalian neurons, a century after Cajal. *Neuron*, **16**, 701–716.